


 CrossMark
 click for updates

 Cite this: *RSC Adv.*, 2014, 4, 46170

Ordered mesoporous V₂O₅/WO₃ composite catalysts for efficient oxidation of aryl alcohols†

 Euaggelia Skliri,^a Ioannis N. Lykakis^b and Gerasimos S. Armatas^{*a}

Multicomponent mesoporous metal oxides show promise in the area of heterogeneous catalysis due to the synergetic interactions between the framework components and the high internal surface area. In this study, we present the synthesis of ordered mesoporous tungsten(vi) oxide–vanadium oxide (V₂O₅) nanocomposite frameworks *via* a two-step wet chemical deposition and nanocasting process and demonstrate that they exhibit high catalytic activity and stability for the oxidation of aryl alcohols, using *tert*-butyl hydroperoxide (*t*-BuOOH) as oxidant. X-ray diffraction, transmission electron microscopy and nitrogen porosimetry results indicate that the template-free materials possess a 3D mesoscopic structure of discernible domains of parallel-arranged nanorods and have an internal pore surface with narrow mesopores. The chemical composition and molecular structure of the mesoporous matrix were determined with elemental X-ray microanalysis (EDS), diffuse reflectance ultraviolet-visible (UV-vis) and Raman spectroscopy. Our catalytic results indicate that a small addition of V₂O₅ into the lattice of WO₃ has a beneficial effect on the catalytic performance. Thus, the 4% V₂O₅-loaded WO₃ catalyst shows a large improvement in the oxidation of various *para*-substituted aryl alcohols with respect to the pure mesoporous WO₃, giving good-to-high yields (*ca.* 80–100%) of the target products within 1–4 h reaction time.

 Received 30th July 2014
 Accepted 11th September 2014

DOI: 10.1039/c4ra07850k

www.rsc.org/advances

Introduction

In recent years, multicomponent metal oxide frameworks perforated by regular arrays of mesopores have attracted a great deal of attention due to their fascinating properties and potential applications in the field of heterogeneous catalysis.¹ This type of porous material represents a significant improvement in the catalytic performance over single-component metal oxides. In addition to the synergetic interactions between the constitutive components of the framework that might induce high catalytic activity and product selectivity,² mesoporosity can provide the desirable highly accessible surface and adequate diffusion of reactants and reaction products to the active sites. Owing to these advantages, many mesoporous mixed metal oxides, such as CuO/CeO₂,³ Au/TiO₂,⁴ and P₂O₅/TiO₂,⁵ have been widely studied as catalysts for a number of chemical reactions including selective oxidation of alcohols and alkanes, oxidation

of CO, reduction of nitro compounds, and degradation of organic pollutants.

Recently, the templated synthesis *via* the nanocasting route has achieved ambiguous success in producing well-ordered mesoporous materials with controllable composition and textural properties.⁶ In general, key steps in this synthetic process involve infiltration of suitable metal precursors within the nanopores of the solid template, thermal decomposition at elevated temperature, and removal of the host matrix by selective etching in aqueous NaOH or HF solution. The resulting mesoporous solids, different from those prepared by conventional sol-gel and co-precipitation routes, possess three-dimensional (3D) nanoscale porous structure with regular size and shape imposed by the template pore morphology. In the last few years, a diverse range of ordered mesoporous metal-oxides, such as Co₃O₄,⁷ Cr₂O₃,⁸ Fe₂O₃,⁹ WO₃,¹⁰ CuO,¹¹ NiO¹² and MnO₂,¹³ and mixed metal-oxides, such as CuFe₂O₄¹⁴ and Cu/CeO₂,^{14,15} with high crystallinity and large surface area have been successfully prepared by using nanocasting method. More recently, we used hard-templating of mesoporous silica to nanocast well-ordered mesostructured frameworks consisting of nanocrystalline metal oxides (*e.g.*, Co₃O₄ and Cr₂O₃) and Keggin-type polyoxometalate clusters (*e.g.*, H₃PW₁₂O₄₀ and H₃PMo₁₂O₄₀).¹⁶ These mesoporous composite materials have a 3D open-pore structure and show great promise in catalytic organic reactions.

^aDepartment of Materials Science and Technology, University of Crete, Heraklion 71003, Crete, Greece. E-mail: garmatas@materials.uoc.gr

^bDepartment of Chemistry, Aristotle University of Thessaloniki, University Campus 54124, Thessaloniki, Greece

† Electronic supplementary information (ESI) available: EDS spectra for x% V₂O₅/WO₃ composites, XRD and N₂ physisorption data for SBA-15 and APS/SBA-15 templates, diffuse reflectance UV-vis spectra and catalytic data for *meso*-WO₃ and x% V₂O₅/WO₃, and catalytic data and N₂ adsorption-desorption isotherms of reused 4% V₂O₅/WO₃ catalyst. See DOI: 10.1039/c4ra07850k

In this study, we present the synthesis and catalytic properties of ordered mesoporous frameworks composed of tungsten(vi) oxide and vanadium oxide (V_2O_5) compounds. As an *n*-type semiconductor with strong acid activity, WO_3 has been successfully used in many catalytic reactions such as hydrodesulfurization of thiophene,¹⁷ isomerization of alkanes¹⁸ and metathesis of olefins.¹⁹ The acid properties of WO_3 have also been employed to improve the selective reduction of NO_x .²⁰ On the other hand, vanadium–tungsten mixed oxides are highly efficient catalysts, widely applied for the selective reduction of NO_x by ammonia²¹ and oxidation of ethanol²² and volatile organic compounds (VOCs)²³ including polychlorinated dibenzofurans (PCDFs).²⁴ Here we demonstrate that mesoporous binary WO_3/V_2O_5 compounds, prepared by a hard template-assisted route, are highly effective and stable catalysts for the oxidation of aromatic alcohols, giving the corresponding carbonyl products in excellent conversion yields (80–100% in 1–4 h). Indeed, the specific mesoporous 4% V_2O_5 -loaded WO_3 catalyst we report shows superior activity compared to non-templated material of the same composition, and pure mesoporous WO_3 .

Experimental

Materials

(3-Aminopropyl)triethoxysilane ($H_2N(CH_2)_3Si(OC_2H_5)_3$, >99%) and anhydrous ethanol (>99.5%) were purchased from Aldrich. Ammonium metavanadate (NH_4VO_3 , >99%) and 12-phosphotungstic acid ($H_3PW_{12}O_{40}$, >98%) were purchased from Alfa Aesar. The weight proportion of water on as-obtained polyoxometalate compound was determined by thermogravimetric analysis (TGA), obtaining a molecular formula of $H_3PW_{12}O_{40} \cdot 26H_2O$. The aryl alcohols used as substrates were of high purity and commercially available from Sigma-Aldrich.

Functionalization of mesoporous silicas

Ordered mesoporous SBA-15 silica was prepared under hydrothermal treatment at 100 °C for 1 day, according to the method reported by D. Zhao *et al.*²⁵ Mesoporous silica functionalized with amine ($-NH_2$) groups was prepared as following: 0.1 g of SBA-15 (dried at 120 °C for 12 h) was dispersed in 50 mL of toluene containing 1.6 mL of (3-aminopropyl)triethoxysilane (APTS). The mixture was left to react at 110 °C for 6 h under reflux conditions and the white powder was recovered by filtration, washed thoroughly with toluene and acetone to remove unreacted APTS, and dried at 80 °C for 18 h to give NH_2 -functionalized silica (APS/SBA-15).

Synthesis of mesoporous V_2O_5/WO_3 composites

In a typical preparation, 0.1 g of APS/SBA-15 hybrid silica was dispersed into an aqueous solution (5 mL) of NH_4VO_3 . The mixture was vigorously stirred for 24 h at room temperature and the obtained solid was isolated by filtration, washed thoroughly with water and ethanol until the eluent became colorless, and dried at 80 °C for 12 h. Then, 0.1 g of the dried product and 0.1 mmol of 12-phosphotungstic acid (PTA) were added in 2 mL of

absolute ethanol inside a vial (20 mL), and the resulting mixture was left under stirring at room temperature until complete evaporation of the solvent (~2 days). The dry powder was heated to 550 °C (1 degree per min ramping rate) for 4 h to decompose the NH_4VO_3 and PTA compounds. Finally, the silica matrix was removed with 2% HF aqueous solution at room temperature to yield ordered mesoporous $x\% V_2O_5/WO_3$ composites. The amount of NH_4VO_3 used in reactions was varied between 24, 52 and 92 mg to give a series of mesoporous $x\% V_2O_5/WO_3$ materials with different loading amount of V_2O_5 , *i.e.* $x = 1, 4$ and 6 wt%, respectively, according to the EDS analysis. Mesoporous tungsten(vi) oxide material (denoted as *meso- WO_3*) was prepared following a similar procedure, but using mesoporous SBA-15 silica as template and without the addition of NH_4VO_3 . For comparative studies, the bulk-like V_2O_5/WO_3 composite (denoted as bulk-4% V_2O_5/WO_3) was also prepared in a similar procedure to 4% V_2O_5/WO_3 , but without using silica template.

Physical characterization

The X-ray diffraction (XRD) patterns were recorded on a PAN-analytical X'Pert Pro MPD X-ray diffractometer (45 kV and 40 mA) using Cu $K\alpha$ radiation ($\lambda = 1.5418 \text{ \AA}$) in Bragg–Brentano geometry. Nitrogen adsorption–desorption isotherms were measured at liquid N_2 temperature (77 K) using a NOVA 3200e volumetric analyzer (Quantachrome, USA). Before analysis, the samples were degassed at 150 °C for 12 h under vacuum ($<10^{-5}$ Torr) to remove moisture. The specific surface areas were calculated using the Brunauer–Emmett–Teller (BET) method on the adsorption data in the 0.08–0.25 relative pressure (P/P_0) range. The total pore volumes were derived from the adsorbed volume at $P/P_0 = 0.95$ and the pore size distributions were obtained by the NLDFT method²⁶ based on the adsorption data. Elemental microprobe analyses were performed on a JEOL Model JSM-6390LV scanning electron microscopy (SEM) system that was equipped with an Oxford INCA PentaFET-x3 energy-dispersive X-ray spectroscopy (EDS) detector. Data acquisition was performed with an accelerating voltage of 20 kV and an accumulation time of 100 s. Transmission electron microscopy (TEM) was performed using a JEOL model JEM-2100 electron microscope operated at an accelerating voltage of 200 kV. Samples were prepared by suspending finely ground powder in ethanol using sonication, followed by depositing a drop of solution onto a Cu grid covered with carbon film. Raman spectroscopy was performed at room temperature using a Nicolet Almega XR micro-Raman spectrometer equipped with a 473 nm blue laser (15 mW) as an excitation source. Diffuse reflectance UV-vis spectra were obtained on a Perkin Elmer Lambda 950 optical spectrophotometer, using an integrating sphere. A $BaSO_4$ powder was used as a 100% reflectance standard and the reflectance data were converted to absorption using the Kubelka–Munk equation: $a/S = (1 - R)^2 / (2R)$, where R is the reflectance and a and S are the absorption and scattering coefficients, respectively.

Catalytic reactions

In a typical experiment, a mixture of substrate (0.1 mmol) and catalyst (50 mg) in 2 mL of acetonitrile (HPLC-grade) was placed in a 4 mL glass reactor sealed with a Teflon cap. The reaction

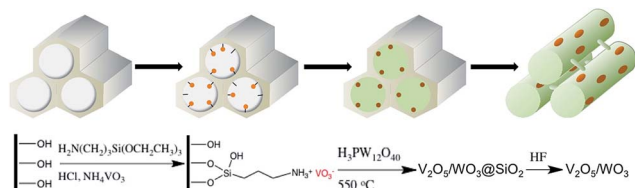
was initiated by adding 40 equivalents of *tert*-butyl hydroperoxide (*t*-BuOOH) and the mixture was vigorously magnetically stirred at 50 °C. The reaction conversion and the products characterization were realized by a combination of gas chromatography-mass spectrometry (Shimadzu GCMS-QP2010 Ultra) and ^1H and ^{13}C NMR spectroscopy (Bruker AMX 300 MHz) by withdrawing small aliquots from the reaction mixture. The spectroscopic data of the products are in agreement with the corresponding commercially available.

Results and discussion

Morphology and structural properties

Ordered mesoporous $\text{V}_2\text{O}_5/\text{WO}_3$ nanocomposite frameworks have been successfully prepared *via* a two-step wet chemical deposition and nanocasting growth of W and V oxides inside an NH_2 -functionalized silica template. In particular, hexagonal mesoporous amino-functionalized silica (APS/SBA-15) is first immersed by pre-treatment in an ammonium metavanadate (NH_4VO_3) solution before the infiltration with 12-phosphotungstic acids. Next, the inorganic precursors are thermally decomposed within the mesopores of APS/SBA-15 template, and the silica matrix was selectively removed by HF etching to leave behind mesoporous V_2O_5 -incorporated WO_3 structure that exhibit different loading amount of V_2O_5 (denoted as $x\%$ $\text{V}_2\text{O}_5/\text{WO}_3$). As we will show the functionalization of the silica surface with aminopropyl groups plays a critical role in the growth of binary structures possessing desired surface composition and, therefore, catalytic properties. Namely, the $-\text{NH}_2$ functionalities can stabilize the NH_4VO_3 precursor within the template mesopores by strong host-guest interactions,²⁷ leading to the formation of a solid solution $\text{V}_2\text{O}_3/\text{WO}_3$ structure, in which the V_2O_3 components are located on or near the surface of nanorods, as illustrated in Scheme 1.

Elemental analysis from energy dispersive X-ray spectroscopy (EDS) on $x\%$ $\text{V}_2\text{O}_5/\text{WO}_3$ products indicated an average atomic ratio of W/V that is consistent with a ~ 1 , ~ 4 and ~ 6 wt% of V_2O_5 loading (x), see Table 1. Note that the EDS vanadium contents are consistently lower than those expected from the stoichiometry of reactions probably due to the insufficient infiltration of NH_4VO_3 compounds into the silica template. However, the present synthetic method is stunningly reproducible and yields mesoporous heterostructures with consistent composition; it was repeated several times giving materials with V_2O_5 loading with less than 15% deviation, according to the EDS results. Notably,



Scheme 1 Schematic representation for the synthesis of ordered mesoporous $x\%$ $\text{V}_2\text{O}_5/\text{WO}_3$ composite materials.

the EDS spectra did not show any signal from silicon, confirming the complete elimination of the silica matrix (see ESI, Fig. S1†).

The mesoporous structure of the templated materials was investigated with low-angle X-ray diffraction (XRD) and transmission electron microscopy (TEM). As indicated by powder XRD (Fig. 1a), the mesoporous tungsten(vi) oxide (*meso*- WO_3) and $x\%$ $\text{V}_2\text{O}_5/\text{WO}_3$ composite solids exhibited a weak but distinct diffraction peak in low-angle range $2\theta \sim 1^\circ$, which according to TEM can be assigned to the (100) reflection of hexagonal $P6mm$ structure. The observation of this diffraction peak clearly suggests a mesoscopic order in these materials, although some deformation of the hexagonal array can be considered due to the low intensity of the (100) diffraction, especially in the 4–6% V_2O_5 -loaded WO_3 samples. On the basis of the hexagonal symmetry and XRD data, it is possible to calculate the lattice constant (a_0) of the pore structure by using the equation $a_0 = (2/\sqrt{3})d_{100}$, where d_{100} is the d -spacing of (100) reflection, and the results are shown in Table 1. These values are almost equal to that of the silica template (*ca.* 10.7 nm, see ESI, Fig. S2†), suggesting good replication of the silica mesostructure.

Fig. 1b presents the wide-angle XRD patterns of the mesoporous *meso*- WO_3 and $x\%$ $\text{V}_2\text{O}_5/\text{WO}_3$ composite samples. It is revealed that the mesoporous products are highly crystallized and exhibit WO_3 monoclinic structure; all XRD patterns can be indexed to a monoclinic cell with lattice constants $a = 7.297 \text{ \AA}$, $b = 7.539 \text{ \AA}$, $c = 7.688 \text{ \AA}$ and $\beta = 90.91^\circ$ (JCPDF card no. 43-1035). The structural assignment based on XRD is also collaborated by TEM and Raman spectroscopy experiments (see below). The XRD patterns did not show any peak due to the crystalline phase of V_2O_5 , implying that vanadium oxide species are uniformly distributed over the WO_3 matrix, although the existence of very small grain size of vanadium oxide particles cannot be excluded.

Typical TEM images of the mesoporous 4% $\text{V}_2\text{O}_5/\text{WO}_3$, in Fig. 2a and b, reveal large domains of parallel arrangement of uniform nanorods, in consistent with the [110] direction of the hexagonal structure. By means of this technique, the nanorods diameter is shown to be ~ 7 nm that is reasonably comparable to the mesopore size of the silica template, ~ 7.4 nm (Fig. S3†). For the investigation of the crystal structure of the 4% $\text{V}_2\text{O}_5/\text{WO}_3$ sample, high-resolution TEM (HRTEM) images and selected-area electron diffraction (SAED) pattern were obtained. HRTEM image taken from a local area of the framework clearly shows well-resolved lattice fringes throughout the nanorods (Fig. 2c) with a d -spacing of 3.8 Å, which is in accordance with the (020)-spacing of monoclinic WO_3 . The image also demonstrated that the nanorods are interconnected to each other with short bridges to form mesostructured superlattices. Fig. 2d depicts the SAED pattern of the 4% $\text{V}_2\text{O}_5/\text{WO}_3$ and shows a series of spotted Debye–Scherrer diffraction rings, suggesting randomly oriented nanocrystals. All these diffraction rings can be readily assigned to the monoclinic phase of WO_3 , in agreement with XRD results.

Fig. 3 displays the N_2 adsorption–desorption isotherms and the corresponding nonlocal density functional theory (NLDFT) plots for mesoporous *meso*- WO_3 and $x\%$ $\text{V}_2\text{O}_5/\text{WO}_3$. All isotherms show type-IV curves with an H_3 -type hysteresis loop,

Table 1 Analytical data and textural properties of mesoporous WO₃ (*meso*-WO₃) and *x*% V₂O₅/WO₃ composite materials

Sample	Atomic ratio ^a (W : V)	V ₂ O ₅ loading (wt%)	Surface area (m ² g ⁻¹)	Pore volume (cm ³ g ⁻¹)	Pore size (nm)	Unit cell (nm)	WT ^b (nm)
<i>meso</i> -WO ₃			22	0.03	4.0, 11.4	10.2	6.2
1% V ₂ O ₅ /WO ₃	97.5 : 2.5	1.0	23	0.04	4.1, 10.7	10.3	6.2
4% V ₂ O ₅ /WO ₃	90.9 : 9.1	3.8	27	0.05	4.5, 10.8	10.3	5.8
6% V ₂ O ₅ /WO ₃	86.5 : 13.5	5.8	37	0.06	4.4, 10.4	10.1	5.7

^a Based on the EDS analysis. ^b The framework wall thickness is given by $WT = a_0 - D_p$, where a_0 is the unit cell size and D_p is the diameter of mesopores.

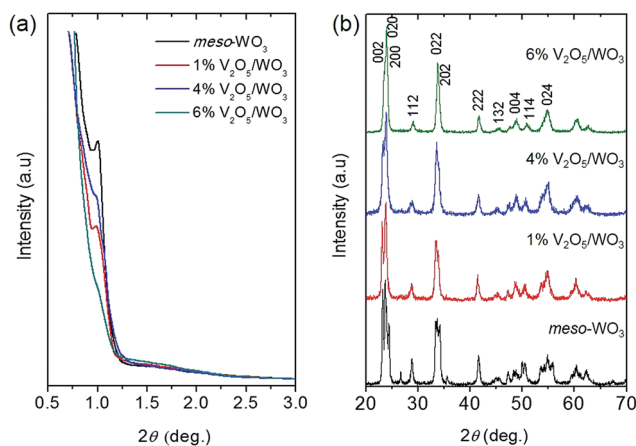


Fig. 1 (a) Small-angle XRD and (b) wide-angle XRD patterns of mesoporous WO₃ (*meso*-WO₃) and *x*% V₂O₅/WO₃ composite materials. These XRD patterns show ordered mesostructure with highly crystalline WO₃ walls.

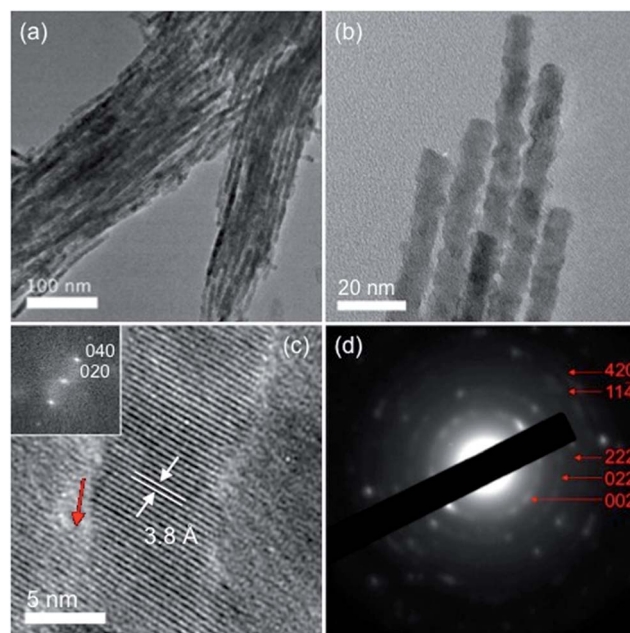


Fig. 2 (a and b) Typical TEM images, (c) high-resolution TEM image and the corresponding FFT plot obtained from a individual nanorod (inset), and (d) selected area electron diffraction (SAED) pattern of mesoporous 4% V₂O₅/WO₃ sample. The red arrow in HRTEM image indicates bridge region between neighboring nanorods.

according to the IUPAC classification, which are attributed to the mesoporous solids with interconnected porosity. In general, the presence of H₃ hysteresis in relative pressure (P/P_0) range 0.4–0.85 is related to the slit-shaped mesopores.²⁸ The adsorption isotherms also exhibit a weak but distinguishable capillary condensation step at relative pressure (P/P_0) \sim 0.2–0.3, indicative of narrow distribution of pore sizes.²⁹ The mesoporous *x*% V₂O₅/WO₃ composites have Brunauer–Emmett–Teller (BET) surface areas in the range of 23–37 m² g⁻¹ and total pore volumes in the range of 0.04–0.06 cm³ g⁻¹. The mesoporous *meso*-WO₃ show a surface area of 22 m² g⁻¹ and a total pore volume of 0.03 cm³ g⁻¹, which are slightly lower than those of composite materials possibly due to the heavier structure of WO₃ (7.2 g cm⁻³) relative to V₂O₅ (3.3 g cm⁻³).

The pore width in as-prepared materials was determined by using the pore size analysis of NLDFT adsorption model for slit-shaped pores, and was found to be \sim 4–5 nm (insets of Fig. 3). This pore size reflects the void space between the interconnected nanorods, which is very close to the framework wall thickness of the SBA-15 template (*ca.* 3.3 nm, see ESI, Fig. S3†). The broad shoulder at 10–11 nm associated the pore size distributions is corresponding to the large voids between the partially interconnected nanorods. From a combination of data from NLDFT and XRD analysis, the pore wall thickness is calculated to be about 6–7 nm, in agreement with TEM analysis.

These results give evidence that the mesoporous products are good replicas of the silica template. Table 1 summarizes the analytical data and the morphological properties of mesoporous *meso*-WO₃ and *x*% V₂O₅/WO₃ composite materials.

The molecular structure of WO₃ and V₂O₅ components in mesoporous matrix was investigated with diffuse reflectance ultraviolet-visible (UV-vis) and Raman spectroscopy. The UV-vis spectra of the as-prepared samples, transformed from the diffuse reflection data according to the Kubelka–Munk theory,³⁰ show a sharp optical absorption onset in the energy range \sim 430–450 nm (\sim 2.8–2.9 eV), which is interpreted by the interband electron transitions in WO₃ (see Fig. S4 of the ESI†). The broad absorption band in the region between 550 and 650 nm appeared in the UV-vis spectra of *x*% V₂O₅/WO₃ composites is assigned to the d–d charge transitions of V₂O₅ species.³¹

Raman spectroscopy is a very efficient technique to probe the crystal structure of WO₃ materials.³² The Raman spectra of *meso*-WO₃ and *x*% V₂O₅/WO₃ materials, shown in Fig. 4, are

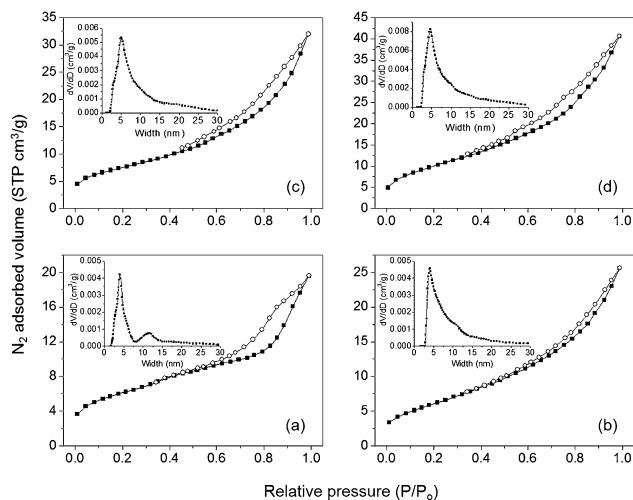


Fig. 3 Nitrogen adsorption–desorption isotherms at 77 K and the corresponding NLDFT pore-size distribution plots calculated from the absorption branch (inset) for mesoporous (a) *meso*-WO₃ and (b) 1% V₂O₅/WO₃, (c) 4% V₂O₅/WO₃ and 6% V₂O₅/WO₃ composite materials.

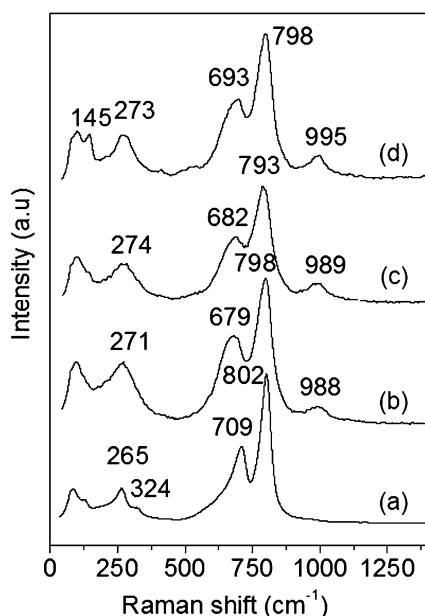


Fig. 4 Raman spectra of mesoporous (a) *meso*-WO₃ and (b) 1% V₂O₅/WO₃, (c) 4% V₂O₅/WO₃ and (d) 6% V₂O₅/WO₃ composite materials.

consistent with the monoclinic phase of WO₃. All spectra displayed intense peaks in 793–802 and 679–709 cm⁻¹ regions that correspond to the W–O–W stretching mode and broad peaks at 324 and 265–273 cm⁻¹ due to the bending modes of O–W–O bonds in the monoclinic WO₃, respectively.^{32,33} Compared to the Raman spectrum of *meso*-WO₃, the W–O–W stretching bands in composite samples shift toward lower wavenumbers, possibly due to the additional formation of W–O–V bonds. The shifts from 120 to 130 cm⁻¹ are attributed to the lattice vibration of crystalline WO₃.³⁴ Clear evidence for the inclusion of V₂O₅ compounds in mesoporous structure comes from the Raman

shift in the region between 988 and 995 cm⁻¹. This peak corresponds to the stretching mode of V=O bonds in the crystalline V₂O₅.³⁵ Prominent blue shift of this band, especially in 6% V₂O₅ loaded sample, may be related with the presence of polymeric vanadia species in the mesoporous structure.³⁶ Taken together with high-resolution TEM images, these results suggest that the pore walls are composed of WO₃ nanocrystals and a small quantity of V₂O₅ compounds.

Catalytic oxidation of aryl alcohols

The catalytic activity of mesoporous x% V₂O₅/WO₃ materials has been evaluated using the oxidation of 1-phenylethanol (**1**) as a probe reaction. All the catalytic reactions were carried out under the same conditions, with 50 mg of catalyst and using *t*-BuOOH as oxidant, at 50 °C. First, the oxidation of **1** was examined with 4% V₂O₅/WO₃ in various solvents. As can be seen in Fig. S5 of the ESI,[†] the acetonitrile was the most suitable solvent for this system, giving 82% yield of acetophenone (**1a**). For comparison, **1** oxidation in toluene and ethanol afforded a significantly lower yield of **1a** under the same conditions, *i.e.* 30% and 29%, respectively. Next optimization was performed for **1** oxidation with 4% V₂O₅/WO₃ catalyst using various amount of *t*-BuOOH oxidant. The conversion yield of **1**, in Fig. S6 of the ESI,[†] indicates that the reaction proceeded to a sufficient yield (85%) in 40 : 1 oxidant-to-substrate molar ratio. Comparatively, a 49% and 83% yield of **1a** was obtained when a 20 : 1 and 50 : 1 ratio of oxidant to substrate was used, respectively.

Having established the optimal reaction conditions for the oxidation of **1**, the compositional dependence of x% V₂O₅/WO₃ mesoporous on catalytic activity was studied. Catalytic results shown in Fig. 5 and Table 2 indicated that V₂O₅ compounds included into the WO₃ matrix have an appealing effect on the catalytic performance. In particular, WO₃ samples loaded with 4–6 wt% V₂O₅ afford a moderate-to-high yield of **1a** (63–89% in 2 h), while the composite material containing lower amount of V₂O₅ (~1 wt%) shows a noticeable drop in activity (55% yield of **1a**). Of

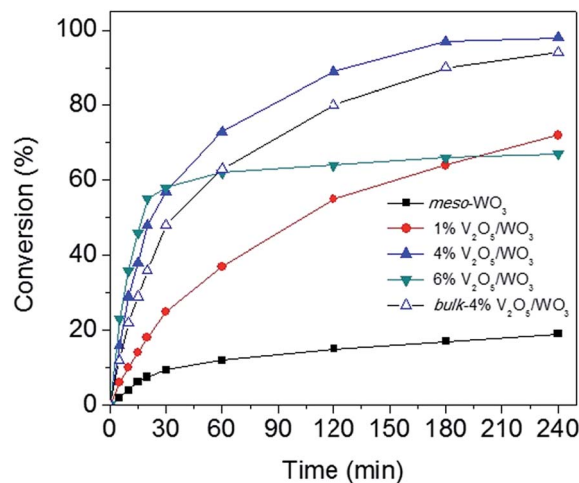


Fig. 5 Time-dependent conversion plots for the oxidation of 1-phenylethanol (**1**) by mesoporous *meso*-WO₃ and x% V₂O₅/WO₃ composite materials and macroscopic bulk-4% V₂O₅/WO₃ solid.

Table 2 Oxidation of 1-phenylethanol (**1**) in presence of *t*-BuOOH catalyzed by mesoporous WO₃ (*meso*-WO₃), *x*% V₂O₅/WO₃ and S-4% V₂O₅/WO₃ materials as well as bulk-4% V₂O₅/WO₃ macroparticles^a

Catalyst	Conversion ^b (%)	Selectivity (%)	Kinetic constant, <i>k</i> (min ⁻¹)
<i>meso</i> -WO ₃	15	100	0.004
1% V ₂ O ₅ /WO ₃	55	100	0.010
4% V ₂ O ₅ /WO ₃	89	100	0.033
6% V ₂ O ₅ /WO ₃	63	100	0.041
S-4% V ₂ O ₅ /WO ₃	84	100	0.021
Bulk-4% V ₂ O ₅ /WO ₃	80	100	0.022

^a Experimental conditions: 0.1 mmol 1-phenylethanol, 50 mg catalyst, 40 equiv. *t*-BuOOH, 2 mL CH₃CN, 50 °C, 2 h. ^b Determined by GC-MS analysis.

particular note, *meso*-WO₃ shows little catalytic activity under the same conditions (*ca.* 15% conv. of **1**, in 2 h). On the basis of **1** consumption, the mesoporous 4% V₂O₅/WO₃ was found to be the best catalyst under the present conditions, giving 89% yield of **1a** in 2 h. Indeed, this catalyst, unlike the other examined materials, catalyzed the oxidation of **1** almost quantitatively to ketone **1a** (~97% yield) within 3 h (see Table 2). Control experiments did not show any significant catalytic activity in the absence of catalyst; the conversion of **1** was less than 3% after 2 h reaction.

The time evolution of the **1** oxidation can be sufficiently described by a pseudo-first-order reaction model. This is reasonable if we account the excess of *t*-BuOOH oxidant, so that its concentration could be considered constant during the reaction. Fig. S7 (ESI[†]) shows the plots of ln(*C_t*/*C₀*) versus time (where *C₀* and *C_t* are the concentrations of **1** at the initial state of reaction and at the time *t*, respectively), by which the apparent first-order reaction rates (*k*) were obtained as a slope of the linear fits. The corresponding *k* values are shown in Table 2. Kinetic analysis indicated that the oxidation reaction proceeds much faster over 4% V₂O₅/WO₃ (0.033 min⁻¹) than the *meso*-WO₃ (0.004 min⁻¹) and 1% V₂O₅/WO₃ (0.010 min⁻¹) catalysts. The 6% V₂O₅/WO₃ although oxidizes **1** at a faster rate (0.042 min⁻¹), it gives moderate conversion yield (~66%) of **1a**. These results indicate that addition of small amount of V₂O₅ into the WO₃ lattice has a beneficial effect of improving the catalytic activity of WO₃. It seems that vanadium oxide is really synergistic catalyst, where WO₃ component is activated by the V₂O₅ species that solid-dissolved in mesoporous matrix. In agreement with this assumption, the W–O–V contribution in composite catalysts is collaborated by Raman spectroscopy.

To examine the role of W–O–V sites on the catalytic performance of V₂O₅/WO₃ materials, we also prepared mesoporous 4% V₂O₅-loaded WO₃ catalyst featuring a V₂O₅-poor surface composition, and then we examined its catalytic activity under similar conditions. This catalyst, designated as S-4% V₂O₅/WO₃, was synthesized by following a procedure similar to that for 4% V₂O₅/WO₃, but using SBA-15 silica as template. The constitution of the non-functionalized silica template used in this experiment is expected to produce mesostructured V₂O₅/WO₃ nanorods in which a certain amount of V₂O₅ will be located to the internal structure. Therefore, this catalyst will possess less V₂O₅

active species accessible to reactants than its modified silica-templated 4% V₂O₅/WO₃ counterpart. Remarkably, the S-4% V₂O₅/WO₃ exhibited lower activity than the corresponding mesoporous 4% V₂O₅/WO₃ sample in oxidation of **1**, giving 84% conversion yield of **1a** in 2 h with a reaction rate constant of 0.021 min⁻¹, see Table 2. This reflects that W–O–V sites on the surface of *x*% V₂O₅/WO₃ eventually contribute to the high catalytic efficiency. Notably, the mesoporous 4% V₂O₅/WO₃ achieves also higher oxidation kinetic as compared to its non-porous analog. For purpose of comparison, we also performed the oxidation experiment on non-templated 4% V₂O₅/WO₃ composite solid, denoted as bulk-4% V₂O₅/WO₃, which is prepared by solid phase sintering of a powder blend containing NH₄VO₃ and 12-phosphotungstic acid compounds; the product shows a BET surface area of 9 m² g⁻¹ and a pore volume less than 0.01 cm³ g⁻¹. Remarkably, the bulk-4% V₂O₅/WO₃ micro-particles although afforded excellent yield of **1a** (~94%) in 4 h, results to less efficient reaction rate (0.022 min⁻¹) that does mesoporous 4% V₂O₅/WO₃ under similar conditions (see ESI, Fig. S7[†]). Such superiority of the mesoporous 4% V₂O₅/WO₃ material may be related to the solid solution of V₂O₅ oxides into the WO₃ lattice, the high crystallinity of WO₃ and the three-dimensional open-pore structure, which offer competitive advantages to the activation of WO₃ structure.

To test the recycling ability of our catalyst, we carried out repeated oxidations of **1** using 4% V₂O₅/WO₃ as catalyst. After each reaction, the catalyst was recovered by simple filtration, washed several times with acetonitrile, and then reused for the next catalytic run. As shown in Fig. 6, the acetophenone (**1a**) yield remained essentially constant (~94–98%) even after four consecutive catalytic cycles, reflecting high durability and reusability of the catalyst. The stability of the mesoporous structure was verified by elemental X-ray microanalysis and N₂ physisorption measurements. EDS spectra indicated no detectable leaching of V₂O₅ after catalysis, showing an average W/V atomic ratio that corresponds to a V₂O₅ content of about 3.6 wt%. Nitrogen adsorption data evidenced no change in the

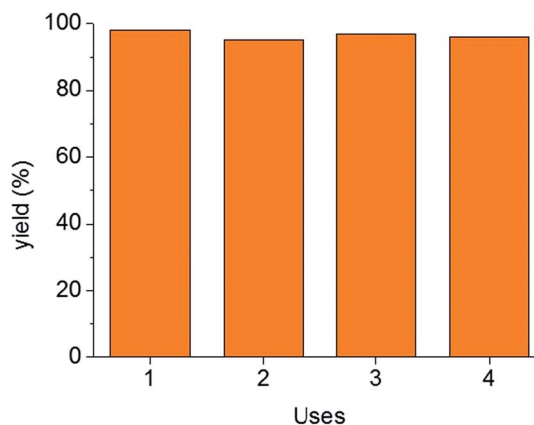


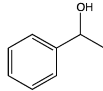
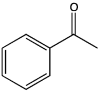
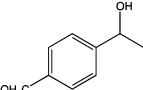
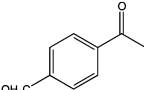
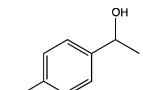
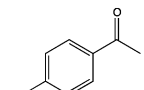
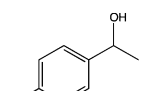
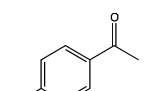
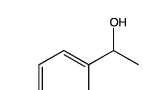
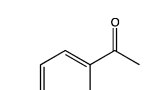
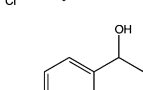
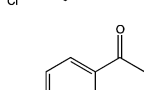
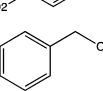
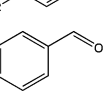
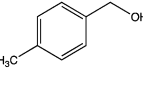
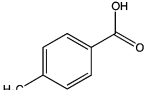
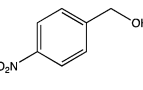
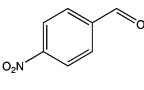
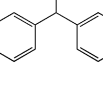
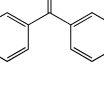
Fig. 6 Recycling of the mesoporous 4% V₂O₅/WO₃ catalyst for the oxidation of 1-phenylethanol (**1**) to acetophenone (**1a**) (experimental conditions: 0.1 mmol 1-phenylethanol, 50 mg catalyst, 40 equiv. *t*-BuOOH, 2 mL CH₃CN, 50 °C, 4 h).

mesoporous structure of reused catalyst compared to the fresh material (ESI, Fig. S8†), indicating a surface area of $26 \text{ m}^2 \text{ g}^{-1}$ and pore volume of $0.05 \text{ cm}^3 \text{ g}^{-1}$. These results consist with high stability and reusability of the 4% $\text{V}_2\text{O}_5/\text{WO}_3$ mesostructure. In addition, the same catalytic reaction was also conducted by using 4% $\text{V}_2\text{O}_5/\text{WO}_3$ catalyst. When the catalyst was separated from the reaction mixture shortly (30 min) and the reaction filtrate was further stirred at 50°C , no additional conversion of **1** was detected by GC-MS analysis even after 2 h; we obtained a $\sim 58\%$ and $\sim 59\%$ conversion yield of **1** before and after removal of the catalyst. These results provide strong evidence that the present oxidation reactions are heterogeneous in nature.

The mesoporous 4% $\text{V}_2\text{O}_5/\text{WO}_3$ efficiently catalyzes the oxidation of various *para*-substituted aromatic alcohols, such as 1-phenylethanols and benzyl alcohols, to their target products.

As seen in Table 3 and Fig. S9a of the ESI,† all the substituted 1-phenylethanols (**2–6**) were oxidized into the corresponding ketones at an almost quantitatively yield ($>97\%$) within 3 h. Also, oxidation of substituted benzyl alcohols (**7–9**) afforded the corresponding aryl aldehydes in a range of 80–94% yields, although in prolonged reaction time (4 h). Of particular note, *p*-methyl benzyl alcohol (**8**) was oxidized into the corresponding *p*-methyl benzaldehyde (**8a**) as the major product (55% conv., 80% relative yield) in 15 min, while at the longer reaction time (3 h) the carboxylic acid (*p*-methylbenzoic acid, **8b**) was formed as the only product. Evidence for this was obtained from GC-MS and NMR spectroscopy. To rule out the possibility of the self-oxidation reaction of aldehyde **8a** to carboxylic acid **8b**, we reacted the aldehyde **8a** with *t*-BuOOH but in the absence of catalyst. In this experiment, only a 8% conversion yield of the *p*-methylbenzoic acid (**8b**) was observed in the reaction mixture

Table 3 Oxidation of various *para*-substituted aryl alcohols **1–10** in presence of *t*-BuOOH by mesoporous 4% $\text{V}_2\text{O}_5/\text{WO}_3$ catalyst^a

	Substrate	Product	Yield ^b (%) / time (h)	Kinetic const., <i>k</i> (min^{-1})
1			97/3	0.033
2			100/1	0.150
3			99/3	0.057
4			98/3	0.051
5			97/3	0.052
6			96/3	0.043
7			80/4	0.025
8			100/3	0.056
9			94/4	0.026
10			99/2	0.041

^a Experimental conditions: 0.1 mmol substrate, 50 mg catalyst, 40 equiv. *t*-BuOOH, 2 mL CH_3CN , 50°C . ^b Determined by GC-MS, with error $\pm 1\%$.

after 2 h, demonstrating that oxidation of aromatic aldehyde to the corresponding carboxylic acid is a catalytic process. These results suggest the strong oxidizing character of the 4% V₂O₅/WO₃ material.

It is noteworthy that the presence of electron-donating or electron-withdrawing group has a moderate effect on the catalytic activation of aromatic alcohols. For example, the electron rich alcohols **2** (X = -OCH₃) reacted to form the corresponding ketone in excellent (>99%) yield in 1 h reaction time. Similarly, alcohols bearing electron-withdrawing substituent such as *p*-bromobenzyl alcohol (**4**), *p*-chlorobenzyl alcohol (**5**) and *p*-nitrobenzyl alcohol (**6**) were oxidized to the corresponding carbonyl compounds with 96–98% conversion. However, the oxidation reaction proceeds slightly faster as the electron-donating ability of the substituent functionality increases, see Fig. S9b of the ESI.† Specifically the pseudo first-order reaction rates, shown in Table 3, indicate an about three times faster kinetic rate for **2** (MeO-substituted) oxidation relative to the oxidation of **3** (Me-substituted), **5** (Cl-substituted) and **6** (NO₂-substituted); $k_{\text{MeO}}/k_{\text{Me}} = 2.6$, $k_{\text{MeO}}/k_{\text{Cl}} = 2.9$ and $k_{\text{MeO}}/k_{\text{NO}_2} = 3.5$. Similar, *p*-methylbenzyl alcohol (**8**) was also oxidized to the corresponding aldehyde (**8a**) in a faster reaction rate (approximately two times) compared to the electron poor alcohols **7** and **9**, *i.e.* possessing the electron-deficient H- and NO₂-groups in *para* position, respectively. It should be stressed that steric properties of the substituent seem to not affect significantly the reaction process. For example, in the case of substrate **10** where the α -substituent is a phenyl group, the rate of the catalytic reaction is about 1.3-times higher to that of **2** alcohol, which contained a methyl group next to the benzylic carbon. These results clearly show that our 4% V₂O₅/WO₃ catalyst is able to catalyze the oxidation of hindered primary and secondary aromatic alcohols with high efficiencies in presence of *t*-BuOOH.

Conclusions

In summary, ordered mesoporous tungsten(IV) oxide and vanadium oxide (V₂O₅) nanocomposite frameworks have been successfully prepared *via* a two-step wet chemical deposition and nanocasting method, using amino-functionalized SBA-15 silica as hard template. X-ray diffraction, transmission electron microscopy and nitrogen physisorption measurements showed that mesoporous V₂O₅/WO₃ heterostructures retain a significant degree of crystalline structure of the silica template, displaying an organized matrix of parallel-arranged nanorods. The elemental composition of the inorganic structure was confirmed by EDS analysis, while the presence of V₂O₅ complexes within the mesoporous matrix was verified with diffuse reflectance UV-vis and Raman spectroscopy. According to these results, the V₂O₅ species dispersed evenly throughout the pore wall, forming a solid-solution structure with WO₃ oxide. The catalytic activity of V₂O₅/WO₃ mesoporous is strongly related to the chemical composition of inorganic framework, with particular relevance of the V₂O₅ content on the surface. Although, pure mesoporous WO₃ and bulk composite V₂O₅/WO₃ microparticles show little activity, mesoporous structures

of V₂O₅/WO₃ composition exhibit high catalytic activity and stability in oxidation of various substituted aryl alcohols. These results point to the great potential of these mesoporous heterostructures in catalytic oxidation reactions.

Acknowledgements

Financial support by the Greek Ministry of Education under Excellence grant (ARISTEIA-2691) and THALES project (MIS 377064) are kindly acknowledged.

Notes and references

- 1 M. A. Carreon and V. V. Gulians, *Eur. J. Inorg. Chem.*, 2005, 27.
- 2 J. Shi, *Chem. Rev.*, 2013, **113**, 2139; H. L. Jiang and Q. J. Xu, *J. Mater. Chem.*, 2011, **21**, 13705.
- 3 W. H. Shen, X. P. Dong, Y. F. Zhu, H. R. Chen and J. L. Shi, *Microporous Mesoporous Mater.*, 2005, **85**, 157; D. Gu, C.-J. Jia, H. Bongard, B. Spliethoff, C. Weidenthaler, W. Schmidt and F. Schüth, *Appl. Catal., B*, 2014, **152–153**, 11.
- 4 A. Corma and H. Garcia, *Chem. Soc. Rev.*, 2008, **37**, 2096; I. Tamiolakis, S. Fountoulaki, N. Vordos, I. N. Lykakis and G. S. Armatas, *J. Mater. Chem. A*, 2013, **1**, 14311.
- 5 D. Li, H. Zhou and I. Honma, *Nat. Mater.*, 2004, **3**, 65.
- 6 A.-H. Lu and F. Schüth, *Adv. Mater.*, 2006, **18**, 1793; Y. Wan, H. F. Yang and D. Y. Zhao, *Acc. Chem. Res.*, 2006, **39**, 423; S. Polarz and M. Antonietti, *Chem. Commun.*, 2002, 2593; D. Gu and F. Schüth, *Chem. Soc. Rev.*, 2014, **43**, 313.
- 7 A. Ruplecker, F. Kleitz, E.-L. Salabas and F. Schüth, *Chem. Mater.*, 2007, **19**, 485.
- 8 K. Jiao, B. Zhang, B. Yue, Y. Ren, S. Liu, S. Yan, C. Dickinson, W. Zhou and H. He, *Chem. Commun.*, 2005, 5618.
- 9 F. Jiao, J.-C. Jumas, M. Womes, A. V. Chadwick, A. Harrison and P. G. Bruce, *J. Am. Chem. Soc.*, 2006, **128**, 12905; B. Tian, X. Liu, H. Yang, S. Xie, C. Yu, B. Tu and D. Zhao, *Adv. Mater.*, 2003, **15**, 1370.
- 10 E. Rossinyol, A. Prim, E. Pellicer, J. Arbiol, F. Hernández-Ramírez, F. Peiró, A. Cornet, J. R. Morante, L. A. Solovyov, B. Tian, T. Bo and D. Zhao, *Adv. Funct. Mater.*, 2007, **17**, 1801.
- 11 X. Lai, X. Li, W. Geng, J. Tu, J. Li and S. Qiu, *Angew. Chem., Int. Ed.*, 2007, **46**, 738.
- 12 F. Jiao, A. H. Hill, A. Harrison, A. Berko, A. V. Chadwick and P. G. Bruce, *J. Am. Chem. Soc.*, 2008, **130**, 5262.
- 13 F. Jiao and P. G. Bruce, *Adv. Mater.*, 2007, **19**, 657.
- 14 H. Yen, Y. Seo, R. Guillet-Nicolas, S. Kaliaguine and F. Kleitz, *Chem. Commun.*, 2011, **47**, 10473.
- 15 L. M. Wan, X. Z. Cui, H. R. Chen and J. L. Shi, *Mater. Lett.*, 2010, **64**, 1379.
- 16 I. Tamiolakis, I. N. Lykakis, A. P. Katsoulidis, M. Stratakis and G. S. Armatas, *Chem. Mater.*, 2011, **23**, 4204; G. S. Armatas, A. P. Katsoulidis, D. E. Petrakis, P. J. Pomonis and M. G. Kanatzidis, *Chem. Mater.*, 2010, **22**, 5739; I. Tamiolakis, I. N. Lykakis, A. P. Katsoulidis, C. D. Malliakas and G. S. Armatas, *J. Mater. Chem.*, 2012, **22**, 6919.

- 17 J. Ramirez and A. Gutierrez-Alejandre, *J. Catal.*, 1997, **170**, 108; R. Thomas, E. M. Van Obers, V. H. J. De Beer, J. Medema and J. A. Moulijn, *J. Catal.*, 1982, **76**, 241.
- 18 V. M. Benitez, C. A. Querini, N. S. Figoli and R. A. Comelli, *Appl. Catal., A*, 1999, **178**, 205; V. Logie, G. Maire, D. Michel and J. L. Vignes, *J. Catal.*, 1999, **188**, 90.
- 19 W. Grunert, E. S. Shpiro, R. Feldhaus, K. Anders, G. V. Antoshin and K. M. Minachev, *J. Catal.*, 1987, **107**, 522; I. Rodriguez-Ramos, A. Guerrero-Ruiz, N. Homs, P. Ramirez de la Piscina and J. L. G. Fierro, *J. Mol. Catal. A: Chem.*, 1995, **95**, 147.
- 20 L. Lietti, J. Svachula, P. Forzatti, G. Busca, G. Ramis and F. Breganic, *Catal. Today*, 1993, **17**, 131.
- 21 P. Forzatti and L. Lietti, *Heterog. Chem. Rev.*, 1996, **3**, 33.
- 22 D.-W. Kim, H. Kim, Y.-S. Jung, I. K. Song and S.-H. Baeck, *J. Phys. Chem. Solids*, 2008, **69**, 1513.
- 23 K. Everaert and J. Baeyens, *J. Hazard. Mater.*, 2004, **109**, 113; S. Albonetti, J. E. Mengou and F. Trifiro, *Catal. Today*, 2007, **119**, 295; S.-Y. Lua, Q.-L. Wang, W. R. Stevens, C. W. Lee, B. K. Gullett and Y.-X. Zhao, *Appl. Catal., B*, 2014, **147**, 322.
- 24 D. Shin, S. Choi, J.-E. Oh and Y.-S. Chang, *Environ. Sci. Technol.*, 1999, **33**, 2657.
- 25 D. Zhao, Q. Huo, J. Feng, B. F. Chmelka and G. D. Stucky, *J. Am. Chem. Soc.*, 1998, **120**, 6024.
- 26 P. I. Ravikovitch, D. Wei, W. T. Chueh, G. L. Haller and A. V. Neimark, *J. Phys. Chem. B*, 1997, **101**, 3671.
- 27 K. K. Zhu, B. Yue, W. Z. Zhou and H. Y. He, *Chem. Commun.*, 2003, 98; Y. Q. Wang, C. M. Yang, W. Schmidt, B. Spliethoff, E. Bill and F. Schüth, *Adv. Mater.*, 2005, **17**, 53.
- 28 S. J. Gregg and K. S. W. Sing, in *Adsorption, Surface Area and Porosity*, Academic Press, London, UK, 1982.
- 29 F. Rouquerol, J. Rouquerol and K. S. W. Sing, in *Adsorption by Powder and Porous Solids. Principles, Methodology and Applications*, Academic Press, 1999.
- 30 P. Kubelka, *J. Opt. Soc. Am.*, 1948, **38**, 448.
- 31 S. Higashimoto, W. Tanihata, Y. Nakagawa, M. Azuma, H. Ohue and Y. Sakata, *Appl. Catal., A*, 2008, **340**, 98.
- 32 A. G. Souza, V. N. Freire, J. M. Sasaki, J. Mendes, J. F. Juliao and U. U. Gomes, *J. Raman Spectrosc.*, 2000, **31**, 451.
- 33 M. B. Najbar, J. Camra, A. Bialas, A. Weselucha-Birczynska, B. Borzecka-Prokop, L. Delevoyeac and J. Klinowski, *Phys. Chem. Chem. Phys.*, 1999, **1**, 4645; C. Santato, M. Odziemkowski, M. Ulmann and J. Augustynski, *J. Am. Chem. Soc.*, 2001, **123**, 10639; F. D. Hardcastle and I. E. Wachs, *J. Raman Spectrosc.*, 1995, **26**, 397.
- 34 G. L. Frey, A. Rothschild, J. Sloan, R. Rosentsveig, R. Popovitz-Biro and R. Tenne, *J. Solid State Chem.*, 2001, **162**, 300.
- 35 T. R. Gilson, O. F. Bizri and N. Cheetham, *J. Chem. Soc., Dalton Trans.*, 1973, 291.
- 36 I. Giakoumelou, C. Fountzoula, C. Kordulis and S. Boghosian, *J. Catal.*, 2006, **239**, 1.